Ferromagnetic clusters and superconducting order in $La_{0.7}Ca_{0.3}MnO_3/YBa_2Cu_3O_{7-\delta}$ heterostructures

P. P. Deen,[1,2] F. Yokaichiya,[3] A. de Santis,[4] F. Bobba,[4] A. R. Wildes,[1] and A. M. Cucolo[4]
[1]*Institut Laue-Langevin, 6 rue Jules Horowitz, Boîte Postale 156, F-38042 Grenoble, France*
[2]*European Synchrotron Radiation Facility, 6 Rue Jules Horowitz, Boîte Postale 220, F-38043 Grenoble, France*
[3]*Brookhaven National Laboratory, P.O. Box 5000, Upton, New York 11973, USA*
[4]*CNR/INFM Supermat Laboratory and Physics Department, University of Salerno, Via S. Allende, Baronissi 84081, Italy*
(Received 18 April 2006; revised manuscript received 6 July 2006; published 14 December 2006)

The existence of magnetic and superconducting order in a $[(La_{0.7}Ca_{0.3}MnO_3)_{100\ \text{Å}}/(YBa_2Cu_3O_{7-\delta})_{100\ \text{Å}}]_{10}$ superlattice has been studied by polarized neutron reflectometry, SQUID magnetometry, and resistivity measurements. The magnetization line shapes observed by SQUID magnetometry under zero-field-cooled and field-cooled conditions imply an inhomogeneously disordered magnetic state of the manganite blocks. This is substantiated by resistivity measurements and polarized neutron reflectometry. Resistivity measurements under field-cooled conditions reveal strong perturbations, which imply that the ferromagnetic $La_{0.7}Ca_{0.3}MnO_3$ blocks contain strong magnetic disorder with perturbations coupled to the magnetic order via charge hopping between domains. Polarized neutron reflectometry under zero-field-cooled conditions, below the superconducting transition, reveal a noncollinear ferromagnetic structure, coherent across half the superlattice blocks. Across the superconducting transition, the noncollinear components are perturbed by the superconducting order and attempt to align with the dominant ferromagnetic order. Additionally, the magnetic correlation length increases from half the superlattice structure to a magnetic structure correlated across the complete superlattice. At temperatures above the superconducting transition, the noncollinear magnetic components and the magnetic correlation length relax to the structure observed below the superconducting transition.

DOI: 10.1103/PhysRevB.74.224414 PACS number(s): 75.70.Cn, 74.45.+c, 74.78.Fk, 28.20.Cz

I. INTRODUCTION

Multilayer superconducting/ferromagnetic (SC/FM) structures are under intense study due to both a fundamental interest and the possible applications in the spintronics industry. Recent advances in the fabrication of heterostructures comprising cuprate and manganite components offer the possibility of spintronic applications involving giant magnetoresistance and high-T_c superconductivity. In fact, giant magnetoresistance (GMR) has recently been observed in trilayers comprising $La_{0.7}Ca_{0.3}MnO_3$ (LCMO) and $YBa_2Cu_3O_{7-\delta}$ (YBCO) components[1] with the GMR effect intrinsically linked to the superconducting state of YBCO. Furthermore, theory predicts a dependence of the superconducting critical current on the spin polarization of the adjacent ferromagnetic blocks,[2] thus offering another degree of freedom for the spintronics industry. Fundamentally these systems are interesting due to their antagonistic ground states, which typically results in the suppression of the superconducting order parameter in close proximity to a ferromagnetic block. However, under certain conditions superconductivity and magnetism are able to coexist. In these cases, this can lead to exotic behavior as a direct result of the proximity effect between superconducting and ferromagnetic phases.[3] In order to study the interactions between ferromagnetism and superconductivity in a systematic approach, it is possible to use artificially grown superstructures comprising ferromagnetic and superconducting blocks. In particular, it is possible to control the magnitude of the exchange interactions by varying the relative thickness of each component. This was initially achieved with BCS superconductors. First, a two-dimensional to three-dimensional variation of the upper critical field was observed with a nonmonotonic dependence of the superconducting transition temperature (T_{SC}) on the thickness of the ferromagnetic layers.[4] Second, an oscillatory T_{SC} is obtained by varying the thickness of the ferromagnetic layers.[5] In these systems, the magnetic blocks would be sufficiently thin to ensure their pair-breaking effect would not destroy the superconducting state. However, recent measurements on Gd/La superlattices have revealed, for the first time, the interplay between 3D superconductivity and magnetism in a superlattice thats exhibit magnetic coupling.[6]

In the previous examples, the ferromagnetic correlation length extends to several thousand angstroms and the correlation lengths of superconducting elemental metals are several hundred angstroms. In contrast, cuprates and transition-metal oxides are characterized by short correlation lengths and these lengths are comparable for the superconducting and ferromagnetic ground states, ξ_{SC} and ξ_{FM}, respectively. Furthermore, ξ_{SC} is highly anisotropic with $\xi_{SC} \sim 3$ Å along the c direction, perpendicular to the CuO_2 planes, and $\sim 10-20$ Å in the a-b plane, parallel to the CuO_2 planes. In contrast, ξ_{FM} is isotropic and ~ 100 Å for transition-metal oxides. The energy scales in these systems are therefore comparable and thus their mutual effects are strongly enhanced.

A strong interplay between superconducting and ferromagnetic order has been observed in LCMO/YBCO superlattices[7] with a suppression of T_{SC} and the Curie temperature (T_c). It was determined that the reduced T_c arose from an inhomogeneous magnetization depth profile due to the suppression of magnetization at the interfaces as a direct consequence of charge transfer between the two materials.[8,9] In addition, polarized neutron reflectometry (PNR) results

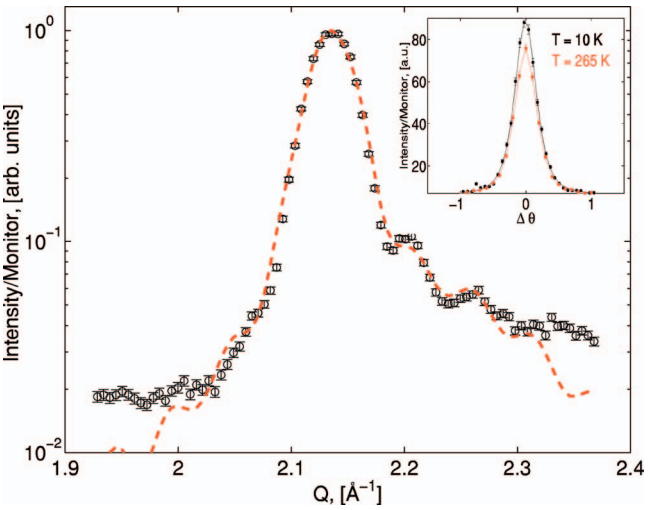

FIG. 1. (Color) Scan of wave-vector transfer around the (0 0 2) reciprocal-lattice reflection. The circles are the experimental data and the dashed line is a fit using the model described by Jehan *et al.* (Ref. 13). Inset: scan of θ around the (1 0 3) Bragg reflection at 265 and 10 K to monitor the moisaicity.

implied either AF magnetization in the YBCO layers or a dead region in the ferromagnetic layer.[10]

In this work, a comprehensive study investigates LCMO/YBCO superlattices via SQUID magnetometry, resistivity measurements, and PNR. The aim is to correlate electronic and magnetic details in these very complex systems. The study focuses on in-plane correlations to probe the long-range magnetic order, typically in-plane for LCMO, and superconducting order where the CuO_2 planes are essential to the development of superconducting order.

II. STRUCTURE

Highly epitaxial single-crystal, $[LCMO_{100\ Å}/YBCO_{100\ Å}]_{\times 10}$, superlattices have been grown by dc sputtering at the University of Salerno.[11] The samples were grown on a $SrTiO_3$ (STO) substrate with the [0 0 1] component in the growth direction. The superlattice structure is deposited directly onto the subtrate with LCMO the first component grown onto the substrate. LCMO, YBCO, and STO have small lattice mismatches, and this makes it possible to grow high-quality single-crystal heterostructures. The lattice parameters, $a=3.881$, $b=3.867$, and $c=5.829$ Å [$c=11.694(2)$ Å], were determined by x-ray diffraction using the (1 0 3), (0 1 3), and the (0 0 2) for the LMCO (YBCO) block Bragg positions. As expected for epitaxial films, the in-plane lattice parameters match the substrate.[12] The mosaicity of the sample as measured at the (0 0 2) position is $0.35\pm0.01°$ [full width at half maximum (FWHM)], and this indicates a high-quality crystalline structure. Figure 1 shows x-ray scattering along the growth direction around the (0 0 2) Bragg reflection. The (0 0 2) reflection is sensitive to the structural correlation of the average bilayer repeat and can be modeled according to the structural model of Jehan *et al.*[13] In this model, the number of planes and the interplanar spacing are allowed to vary and a tanh function is used to represent the variation of concentration and d-spacing at the interface. The dashed line in Fig. 1 is the fit to a model for an average bilayer with YBCO thickness$=129\pm1$ Å, LCMO thickness$=105\pm1$ Å, and an interface roughness of 2 atomic layers. Scans of wave-vector transfer along $[H\ 0\ 0]$ and $[0\ K\ 0]$ give in-plane correlation lengths of $\xi=850$ and 350 Å, respectively, while the out-of-plane correlation length is restricted to the individual blocks.

The inset of Fig. 1 shows a scan around the (1 0 3) Bragg reflection at 265 and 10 K. The mosaic spread and intensities are equivalent for the two temperatures, thus indicating that there is no increased strain in the systems as a result of poorly matched thermal parameters of the three components in the superlattice.

III. RESISTIVITY

Superconducting order was established via resistivity measurements using the four-probe method taking special care to remove any external influences through the use of a lock-in amplifier. Measurements were performed under zero-field-cooled (ZFC) and field-cooled (FC) conditions with the sample cooled in zero external field to base temperature for ZFC and cooled in a small field, $H\sim50$ Oe, before measuring the FC state.

The ZFC resistivity line shape, given in Fig. 2(a), clearly shows the LCMO metal to insulator (M-I) transition $T_P\sim175$ K. In contrast, Pietro *et al.*[14] did not observe a M-I transition for LCMO blocks with a thickness of 4 unit cells and assigned this to the two-dimensional character of the LCMO blocks. The M-I transition observed in this work under ZFC conditions would therefore imply the three-dimensional character of the LCMO blocks. The ZFC resistivity line shape also clearly shows the superconducting transition, T_{SC}, of the YBCO blocks, $T_{SC}=69\pm1$ K. The relative width of the superconducting transition is broad, $\Delta T=5$ K, and reflects imperfections within the superlattice structure with respect to a perfect crystal. The low value of T_{SC} found for these superlattice structures can originate from either a low oxygen stochiometry or a dimensionality effects. T_{SC} of bulk YBCO has a strong dependence on oxygen content.[15] In a bulk sample, $T_{SC}=69$ K would indicate a deficient oxygen content of approximately 6.78 per unit cell. This is also reflected in the lattice parameter with a c-lattice parameter equal to 11.700 Å, close to the lattice parameter observed 11.694 Å, corresponding to an oxygen content of 6.78 per unit cell.[15] However, the strain imposed by the substrate and the components of the heterostructure alters these values. In particular, T_{SC} varies with YBCO thickness and a variation of $T_{SC}\sim35.5$ K to bulk T_{SC}, ~89 K has been observed by the crystal growers for film thickness between 3 unit cells and 300 Å, approximately 26 unit cells, respectively.[16] Equally, a study of LCMO/YBCO superlattices with 15 unit cells of LMCO revealed that an increase of YBCO thickness from 3 to 15 unit cells results in a change in T_{SC} from 20 K to the bulk value.[17] As such, in this study with YBCO blocks comprising 11 unit cells, T_{SC} would be expected to reach the bulk value. Therefore, with such reasoning, the origin of the low T_{SC} value can be ascribed to a

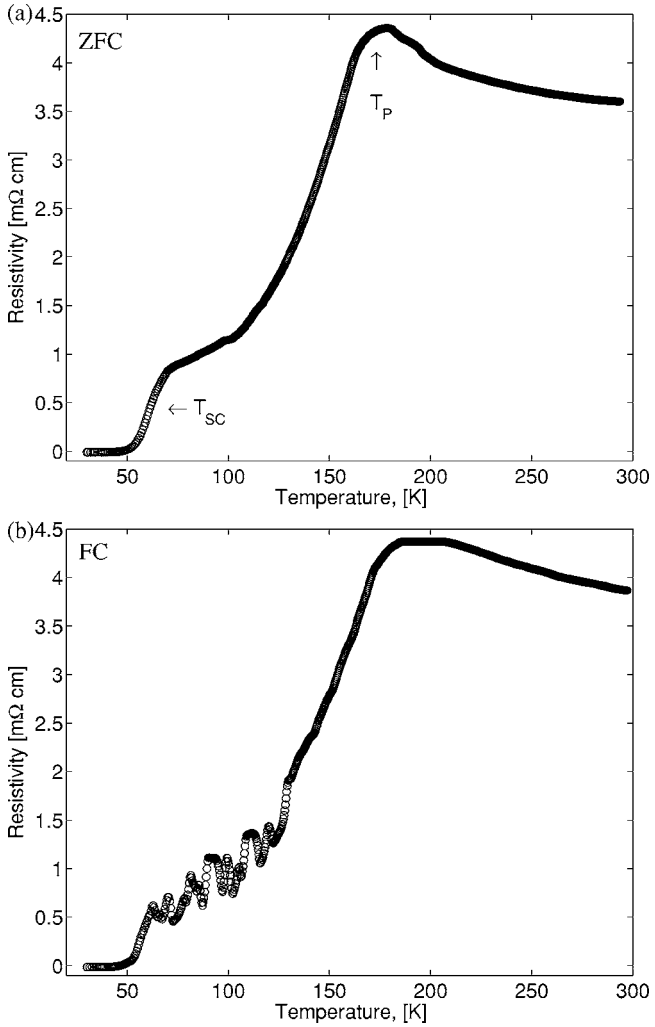

FIG. 2. (a) ZFC resistivity measurements showing the LCMO M-I transition and the YBCO superconducting transition. (b) FC resistivity measurements with $H_{applied}$=50 Oe. Large perturbations are assigned to a conductive phase separation within the LCMO blocks. The flattening of the resistivity line shape is due to overload effects.

small deficiency of oxygen stoichiometry. Unfortunately, such reasoning is incorrect since oxygen stoichiometry also affects the atomic positions in the YBCO unit cell, and it has been demonstrated that an oxygen deficiency leads to a reduced distance between the two CuO_2 planes[18] for single crystals. In the case of thin film or superlattice samples, the distance between the CuO_2 planes, variable through the strain in the heterostructure, varies T_{SC} in precisely the same manner that deoxygenation varies T_{SC}.[19] It is therefore difficult in this study to determine the exact origin of the reduced T_{SC} value.

The FC resistivity, measured with $H_{applied}$=50 Oe in the a/b plane, is shown in Fig. 2(b). Although the M-I transition remains a clear feature, this transition is broader than under ZFC conditions. Below 150 K, strong perturbations in the resistivity appear. These fluctuations disappear below T_{SC}. Noise in resistivity line shapes has been observed in LCMO thin films grown on STO substrates[20] and has been explained in terms of the percolation effect. It was shown that in some parts of the manganite phase diagram, there may be percolationlike transitions between more and less conductive phases that would lead to fluctuations in the resistance. These phases may be electrical or magnetic in origin. Each state has a different conductivity and thus makes a different contribution to the overall conductivity. The percolation effect has been used to describe the M-I transition where the transition occurs via such a multiphase state. As such, the fluctuations would be strongest around the M-I transition. However, strong interactions between the spin and lattice in manganites can give rise to an inhomogeneous charge distribution even in the metallic phase. Thus, the fluctuations can be coupled to the magnetization, and this has been explained in terms of charge hopping between domains in an inhomogeneous disordered magnetic material.[20,21] It was suggested[22] that the electrons may be localized in ferromagnetic wave packets and the current at low temperature is transported by zero point hopping of the carriers between these packets across barriers that are associated with canted spins. The magnetic structure in this case is likened to an ensemble of ferromagnetic clusters in a paramagnetic matrix resembling a spin glass. Additionally, ferromagnetic clusters distributed in an antiferromagnetic matrix are also reported for several electron-doped manganites,[23–25] and for certain concentrations this can lead a strongly frustated magnetic state.[26] The magnetic moment observed in such systems is greatly reduced in comparison to the moment of Mn in the fully ordered ferromagnetic state.

The origin of the resistance noise can be characterized by its dependence on applied magnetic field and via its frequency domain.[21,27,28] Wirth *et al.*[21] determined that the mean fluctuating lifetime would have a strong dependence on the applied magnetic field,

$$\tau_l = \tau_{0,l} \exp \frac{E_l(H=0) + (m_l - m_w)H}{k_B T}. \quad (1)$$

E_l is the energy barrier of the state, m_l and m_w are the magnetic moments of the two states of the fluctuator and at the energy barrier separating the two states, and k_B is Boltzmann's constant. Wirth *et al.*[21] found E_l=23±2 meV, $\tau_{0,l}=3.11\times10^{-11}$ s, and $m_l - m_w \sim 550\mu_b$ for bulk $La_{0.7}Ca_{0.3}MnO_3$. According to Eq. (1), the mean fluctuating lifetime, τ_l, for 50 Oe is three orders of magnitude faster than that observed for 200 Oe. The random nature of the fluctuations makes it difficult to determine an absolute fluctuating lifetime. Nevertheless, Fig. 3 clearly shows that the mean lifetime of the fluctuations is greaty enhanced with the application of a larger magnetic field.

The random nature of resistivity noise results in large variations between equivalent samples,[21,28] and although it is difficult to determine a mean fluctuating lifetime, it is nevertheless possible to ascertain the frequency content of the resistance fluctuations via Fourier transformation. Resistance noise due to magnetic domain fluctuations in manganites typically show a $1/f$, f=frequency, spectral power dependency.[27,29] Figure 4(a) reveals the frequency domain of the resistivity line shapes of Fig. 2 for an applied field of (a)(i) 50 and (a)(ii) 200 Oe across a range of temperatures.

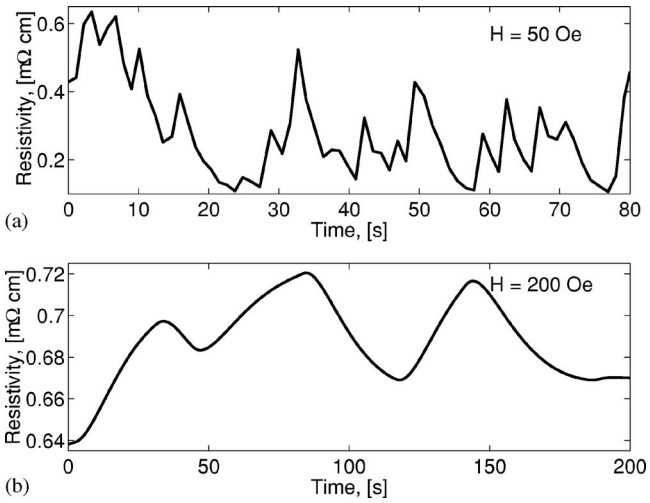

FIG. 3. Time dependence of the resistivity fluctuations under the application of (a) 50 Oe and (b) 200 Oe at 100 K.

The frequency indeed shows a $1/f$ power-law dependence with a large increase in spectral power for smaller frequencies. The variation in temperature, from 128(1) to 74(2) K in the case of 50 Oe and from 114(2) to 89(2) K in the case of 200 Oe, does not substantially alter the spectral power. However, the application of an increased applied magnetic field gives rise to a broader frequency spectrum with diminished spectral power. Hence the scattering centers that lead to the resistance noise do not alter with temperature but are strongly affected by a magnetic field. The large variations in spectral density with temperature are rather strange and require further study.

The temperature dependence of the total spectral power for 50 and 200 Oe, Fig. 4(b), is greatly enhanced below 150 K and becomes negligible below $T \sim 50$ K for both applied fields. We do not assign these fluctuations to strain effects within the superlattice since they become substantial below 150 K and we see, via the mosaicity and intensity of the (0 0 2) Bragg peak, that the strain does not vary greatly with temperature.

Resistance noise originating from the M-I transition via the percolation mechanism is expected to be present in a small region surrounding the M-I transition.[27] However, in several manganite systems, including this study, resistance noise has been observed over a large temperature range.[20,21] In particular, the study by Wirth *et al.*[21] reveals resistivitiy noise in the range $167 < T < 15$ K for thin films of $La_{2/3}Ca_{1/3}MnO_3$. This is possible for a system with an inhomogeneous magnetic state, even at low temperatures, in which the conductive properties of the different phases lead to resistance noise. In fact, a μSR study on $Gd_{0.08}CaySr_{0.92-y}MnO_3$ ($y > 0.5$) revealed an inhomogeneous distribution of the internal magnetic field even at 5 K.[30] These data, with the corresponding analysis and comparison with previous manganite studies, infer a magnetic origin of the resistance fluctuations in these superlattice systems. The magnitude of such noise can increase dramatically as a function of structural disorder and strain, and this could be the origin of the large variations in spectral density with temperature. Further investigations of the conductive properties of LCMO/YBCO heterostructures are required to fully understand this behavior.

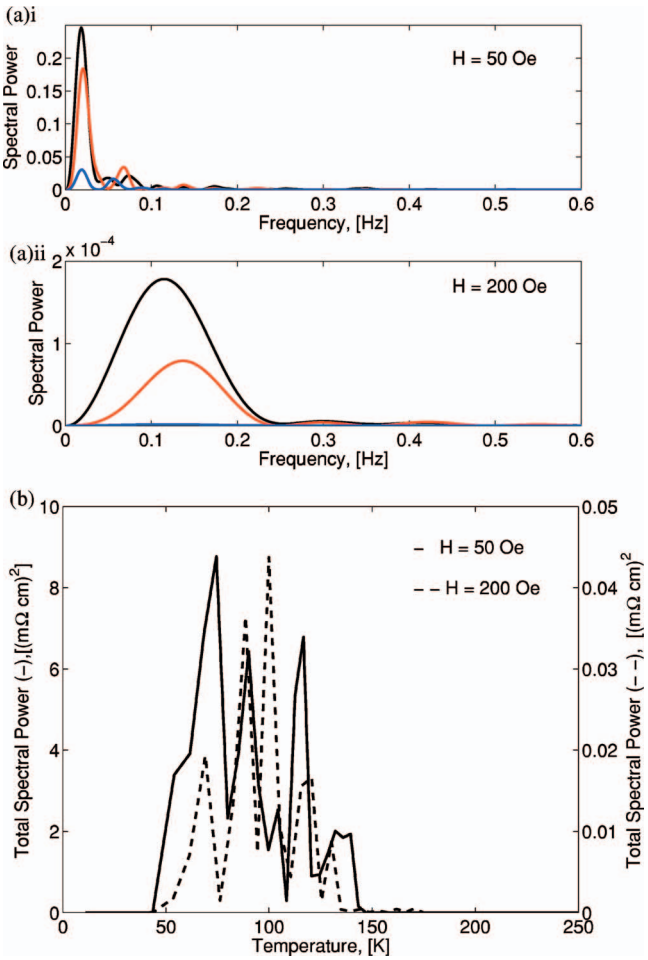

FIG. 4. (Color) (a) Fourier domain of the fluctuating resistivity, spectral power in units of $(m\Omega\,cm)^2$. As observed in Fig. 3 under applied field (a)(i) 50 Oe [128(1) K, 116(2), and 74(2) K] and (a)(ii) 200 Oe [114(2), 115(2), and 89(2) K]. (b) shows the total spectral power of the Fourier transform as a function of temperature.

IV. MAGNETIZATION

dc magnetic susceptibility was measured using a SQUID magnetometer (Quantum Design MPMS) at the University of Liverpool and at the CNRS, Grenoble. Figure 5 shows the ZFC and FC magnetization line shapes with a field of 30 Oe in the *a-b* plane.

A ferromagnetic transition corresponding to the ordering of the LCMO blocks occurs at $T_c = 197 \pm 5$ K for both the FC and ZFC curves. This is a depressed value in comparison to bulk LCMO with T_c reported in the range of 230–260 K.[31] The magnetization curve of the FC state is typical for ferromagnetic LCMO and indicates a saturation magnetization of $0.059(2)\mu_B$/Mn, a much reduced value from the saturation moment for bulk Mn, $3.64\mu_B$/Mn. A small value for the magnetic moment has previously been observed in LCMO/

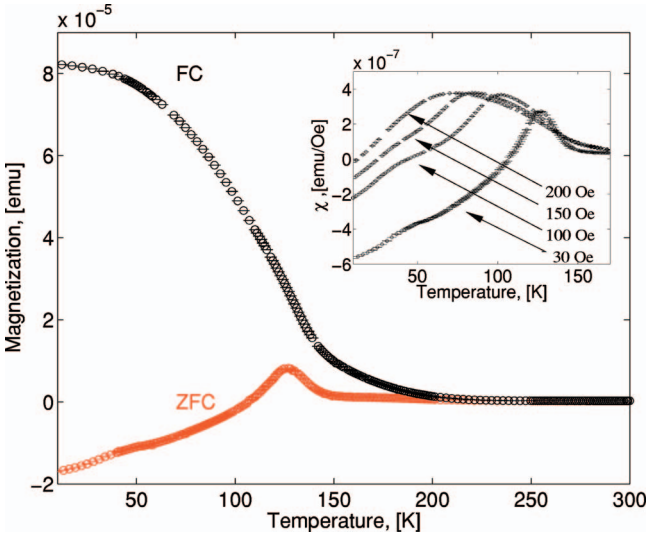

FIG. 5. (Color) Temperature dependence of the magnetization under FC and ZFC conditions. $H_{\text{applied}}=30$ Oe along the a-b plane of the sample. The inset shows the dependence of the ZFC curve under increasing applied field when measuring from base temperature to 300 K.

STO superlattices, $0.12\mu_B$/Mn, and was attributed to the epitaxial strain and/or dead layers arising from surface or interface disorder.[32] An equally small magnetic moment has been observed in LCMO/YBCO superlattices[9] and was attributed to charge transfer between the two materials.

There is a marked contrast between the FC and ZFC magnetization line shapes. In the ZFC line shape here are two perturbations in the ZFC magnetization line shape. The first perturbation around $T\sim 120$ K is reminiscent of antiferromagnetic order and thus appears to mimic the behavior of Gd/La superlattices where long-range 3D superconducting order in the La blocks coexists with antiferromagnetic ordering of ferromagnetic Gd blocks.[6] However, the maximum of the ZFC curve, inset of Fig. 5, is strongly field-dependent. This is typical of a spin glass or the ferromagnetic clusters of mictomagnetic order.[33] PNR was essential to differentiate between antiferromagnetic ordering of the LCMO blocks and a less homogeneous magnetic state.

V. POLARIZED NEUTRON REFLECTOMETRY

PNR has been performed using D17 at the Institut Laue-Langevin. The magnetic scattering cross section for neutrons is comparable to the nuclear cross section, making neutron scattering an ideal tool in the investigation of magnetic structures. Additionally, by probing the change in the polarization state of the neutron upon scattering, it is possible to separate the nuclear from the magnetic cross section, and magnetic moment directions can be directly determined.[34] In the scattering geometry, employed for reflectivity, the wave-vector transfer $\mathbf{Q}=\mathbf{k_f}-\mathbf{k_i}$ is perpendicular to the basal plane and parallel to the growth direction. Hence the magnetization profile along the growth direction perpendicular to the a/b plane is probed. PNR provides four scattering cross sections, which shall be denoted $R++$, $R--$ for non-spin-flip (NSF) scattering and $R+-$, $R-+$ for spin-flip (SF) scattering. NSF cross sections are sensitive to $\vec{\mu}\|\mathbf{H}$ and $\vec{\mu}\perp\mathbf{Q}$ while SF cross sections are sensitive to $\vec{\mu}\perp\mathbf{H}$ and $\vec{\mu}\perp\mathbf{Q}$. The sample was mounted in a variable temperature cryostat. ZFC conditions were achieved by cooling the sample in zero field before applying a small guide field along the a/b plane providing $H\sim 50$ Oe on the sample. FC conditions were achieved by cooling in the small guide field. All the experiments mentioned in this work have been performed on the same original sample to ensure that the datasets between different probes were comparable. The original sample surface area measured 10×10 mm^2. The sample had been cleaved for the SQUID measurements and PNR was performed on the remaining sample with a surface area 5×10 mm^2. PNR measurements were performed across T_{SC} at 5, 45, 68, and 100 K and furthermore under FC conditions at 5 K.

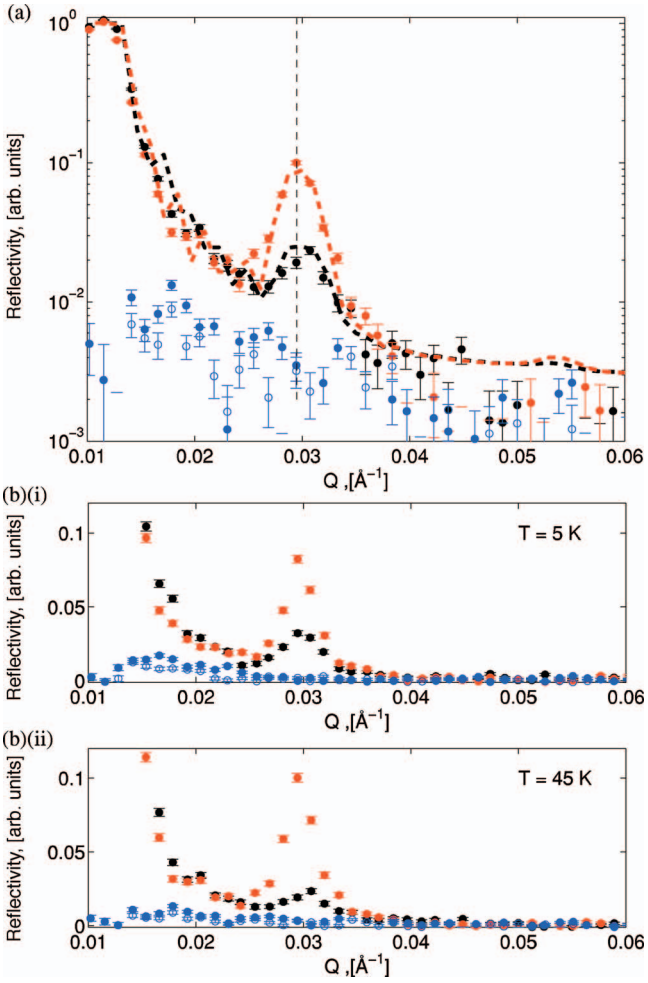

FIG. 6. (Color) PNR under ZFC conditions at (a) 45 K showing the ○ $R--$, ○ $R++$, and ○ $R+-$, $R-+$ cross sections. The red and black dashed lines are a fit to the data. The vertical dashed line indicates the position of the first structural Bragg peak. (b) Reflectivity data plotted on a linear scale to show clearly the behavior of the non-spin-flip scattering cross section for (i) ZFC 5 K and (ii) ZFC 45 K.

Figure 6(a) shows the reflectivity curves obtained at 45 K ZFC. All data have been corrected for supermirror and flipper efficiencies.[35] The vertical dashed line in Fig. 6(a) indi-

cates the position of the first structural Bragg peak, and at this position a large difference in scattering intensity of the NSF scattering is observed indicating strong ferromagnetic order in the a/b plane. The SF scattering is very broad in $\mathbf{Q}$ and shows no Bragg peaks. This is in agreement with results observed by Hoffmann *et al.*[9] Further details regarding the SF scattering are described in a later paragraph.

The red and black dashed lines of Fig. 6(a) are a fit to the data using a simple model with in-plane ferromagnetic ordering of the LCMO blocks. In this model, the LCMO blocks are correlated across the complete superlattice along the c direction.[36] The fit determines a magnetic moment of $0.065(5)\mu_B$/Mn atom. Such a small moment is supported by the negligible difference in the critical angle of the reflectivities $R++$ and $R--$. In addition, the magnitude of the moment is comparable to that found by SQUID magnetometry, $0.059(2)\mu_B$/Mn in the FC phase. The small magnetization magnitude is consistent with ferromagnetic clusters in a randomly oriented magnetic matrix. In this work, the magnetization of the LCMO blocks is 90 emu/cm^3. This is indeed much smaller than that observed by Moon-Ho *et al.*[32] for a 250-Å thin film on an STO substrate, 400 emu/cm^3, but is equivalent to a multilayer sample comprising a [25 Å(LCMO)/70 Å(STO)]$_3$ multilayer that showed 150 emu/cm^3. Moon-Ho *et al.* assign the loss of magnetization to magnetic disorder at the interfaces. PNR is sensitive to the correlation length of the magnetic order along the growth direction, and these data reveal that a small moment exists throughout the LCMO blocks, not just at the interfaces. These data thus indicate an inhomogeneous order of the LCMO blocks leading to a small magnetization value.

Reflectivity data are historically shown on a logarithmic scale. The small deviations observed in these data sets require closer analysis, and this is possible on a linear scale as shown in Fig. 6(b) for (i) 5 K and (ii) 45 K. The SF scattering of Fig. 6(b), sensitive to components in the a/b plane but perpendicular to the applied magnetic field, shows a weak scattering cross section above the background that extends over a long range in $\mathbf{Q}$. In fact, the scattering extends to $\mathbf{Q}\sim 0.04$ Å^{-1}. This scattering can be assigned to short-range in-plane order perpendicular to the dominant ferromagnetic component. An unusual aspect of the SF scattering cross sections is the nonequivalence between $R+-\neq R+-$ for 5 K but not observed at 45 K. Within the kinematic theory of neutron scattering, $R+-=R+-$. Evidently this is not an issue with corrections performed on these datasets since these variations are observed between datasets upon which the same corrections have been applied. At present this issue is unresolved, but it appears likely that this is intrinsic to neutron reflectometry and is under investigation.

The variations in intensities and line shapes of the NSF scattering are small across the superconducting transition, and within statistical error the fit obtained for the ferromagnetic model in ZFC at 45 K, Fig. 6(a), is adequate for all temperatures. It is therefore impossible to determine with certainty the existence of a dead layer at the YBCO/LCMO interface or an antiferromagnetic component in the YBCO blocks by modeling the reflectivity profiles. Instead, more information is gained by fitting a Gaussian line shape with a $\mathbf{Q}^{-4}$ background across the NSF magnetic components. In this manner, the magnetic intensities, $(R-)-(R++)$, and correlation lengths, $\xi=2\pi/\Delta\mathbf{Q}$, can be determined. Figure 7 shows the variation of these parameters across the superconducting transition in the ZFC phase.

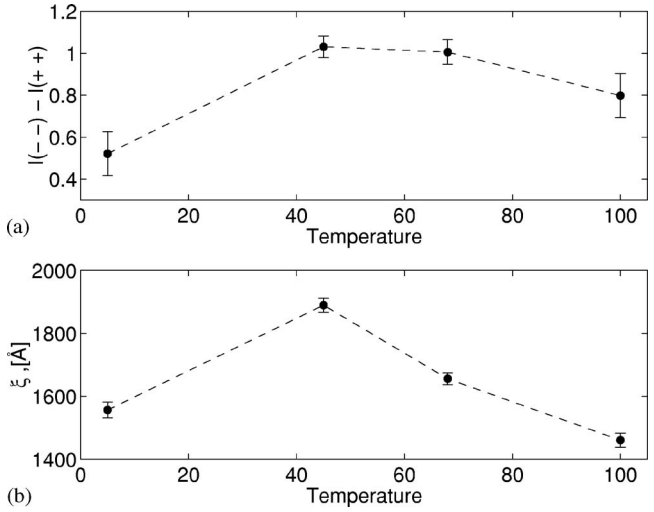

FIG. 7. (a) $(R-)-(R++)$ components across T_{SC}, (b) variation of ferromagnetic correlation length.

The magnetic intensities observed correspond to the magnetic components parallel to the guide field and perpendicular to $\mathbf{Q}$. Figure 7(a) clearly shows the perturbation of this component across the superconducting transition. At 5 K, the magnetic order is correlated across half the superlattice structure. Across the perturbation observed by SQUID magnetometry, $T\sim 45$ K, the noncollinear components rotate to align ferromagnetically, and this structure is correlated throughout the superlattice. The noncollinear components return as the temperature is increased beyond T_{SC} and the magnetic order is again only correlated across half the superlattice structure. It is thus clear that the magnetic order of the LCMO propagates across the YBCO blocks and that their mutual interaction leads to a rearrangement of the magnetic state.

The magnetic structure was also probed in the FC state. Figure 8 compares the NSF $R++$ scattering observed under FC conditions at 5 K with $R++$ scattering under ZFC conditions at 45 K and shows equivalent magnetic states under both conditions.

The PNR results underline that the variation in the magnetization line shape, observed in Fig. 5, is not due to a large rearrangement of magnetic order. Instead, the line shapes are due to a noncollinear, spin-glass-type structure that aligns under a small external field but remains disordered under ZFC conditions. The perturbation at 120 K in Fig. 5 can therefore be asigned to the blocking temperature of the spins. The substantial variation in magnetization line shapes combined with the spatial information gained from PNR would indicate that this effect occurs not only at the interfaces but throughout the system. In addition, PNR has revealed that the onset of superconducting order gives rise to a perturbation of the noncollinear moments in the LCMO blocks.

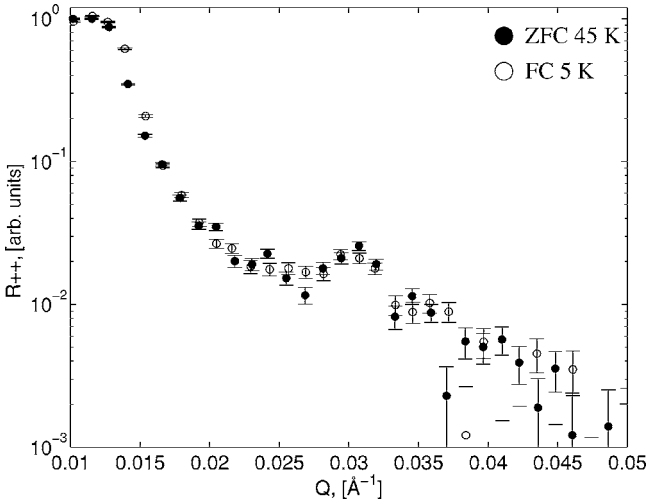

FIG. 8. NSF R++ line shape for ZFC 45 K and FC 5 K.

VI. DISCUSSION

In conclusion, the magnetic and electronic state of an LCMO/YBCO superlattice has been probed by SQUID magnetometry, resistivity, and PNR. The experimental results indicate the coexistence of a long-range noncollinear inhomogeneous magnetic state within the plane of the LCMO blocks with superconducting order within the YBCO blocks. Strong fluctuations in resistivity measurements are explained in terms of charge hopping between ferromagnetic domains in the LCMO blocks. The magnetic order in the LCMO blocks can therefore be seen as an ensemble of noncollinear ferromagnetic clusters. This is reflected by the magnetization line shapes, obtained under FC and ZFC conditions, which resemble the line shapes observed for spin-glass or mictomagnetic order. PNR indicates a dominant in-plane ferromagnetic state in the LCMO blocks for both ZFC and FC states, which are correlated across the superconducting YBCO blocks. However, the magnitude of the magnetic moment is very small in comparison to bulk LCMO. In order to determine the origin of the reduced moment, the effects of shape anisotropy or the possibility of charge transfer between the two materials LCMO and YBCO has not yet been addressed. The notion of noncollinear magnetic domains is strengthened by the interplay between magnetic order and superconductivity. Across the superconducting transition, the noncollinear magnetic domains are perturbed by the superconducting order and align parallel to the in-plane ferromagnetic components. Additionally, the magnetic order extends from half the superlattice structure to the complete heterostructure across the superconducting transition. Below and above T_{SC}, the magnetic structure relaxes to the state of greater noncollinearity. These results directly demonstrating the proximity effect between the superconducting and ferromagnetic correlation lengths.

The behavior exhibited by LCMO/YBCO superlattices is reminiscent of ruthenocuprate superlattices where the interplay between high T_c superconductivity and magnetism coexists with spin-glass-like behavior.[37,38] LCMO/YBCO superlattice structures can therefore shed new light on the intricate coupling of unconventional superconducting order.

[1] V. Peña, Z. Sefrioui, D. Arias, C. Leon, J. Santamaria, J. L. Martinez, S. G. E. teVelthuis, and A. Hoffmann, Phys. Rev. Lett. **94**, 057002 (2005).
[2] A. I. Buzdin, A. V. Vedyayev, and N. V. Ryzhanova, Europhys. Lett. **48**, 686 (1999).
[3] Y. Izyumov, Y. Proshin, and M. Khusainov, Phys. Usp. **45**, 109 (2002).
[4] H. K. Wong, B. Y. Yin, H. Q. Yang, J. B. Ketterson, and J. E. Hilliard, J. Low Temp. Phys. **63**, 307 (1986).
[5] J. S. Jiang, D. Davidović, D. H. Reich, and C. L. Chien, Phys. Rev. Lett. **74**, 314 (1995).
[6] P. P. Deen, J. P. Goff, R. C. C. Ward, M. R. Wells, S. Langridge, S. Dalgliesh, S. Foster, and G. J. McIntyre, J. Phys.: Condens. Matter **17**, 3305 (2005).
[7] H. U. Habermeier and G. Cristiani, Phys. Status Solidi A **201**, 1436 (2004).
[8] T. Holden, H. U. Habermeier, G. Cristiani, A. Golnik, A. Boris, A. Pimenov, J. Humlícek, O. I. Lebedev, G. VanTendeloo, B. Keimer, and C. Bernhard, Phys. Rev. B **69**, 064505 (2004).
[9] A. Hoffmann, S. G. E. teVelthuis, Z. Sefrioui, J. Santamaria, M. R. Fitzsimmons, S. Park, and M. Varela, Phys. Rev. B **72**, 140407(R) (2005).
[10] J. Stahn, J. Chakhalian, C. Niedermayer, J. Hoppler, T. Gutberlet, J. Voigt, F. Treubel, H.-U. Habermeier, G. Cristiani, B. Keimer, and C. Bernhard, Phys. Rev. B **71**, 140509(R) (2005).
[11] M. Salvato, A. Vechionne, A. D. Santis, F. Bobba, and A. M. Cucolo, J. Appl. Phys. **97**, 103712 (2005).
[12] A. de Andrés, G. Castro, S. Taboada, J. L. Martínez, and J. M. Colino, Appl. Phys. Lett. **83**, 713 (2003).
[13] D. A. Jehan, D. F. McMorrow, R. A. Cowley, R. C. C. Ward, M. R. Wells, N. Hagmann, and K. N. Clausen, Phys. Rev. B **48**, 5594 (1993).
[14] M. V. P. Prieto, P. Vivas, G. Campillo, E. Baca, L. F. Castro, M. Varela, C. Ballesteros, J. E. Villegas, D. Arias, and C. León, J. Appl. Phys. **89**, 8026 (2001).
[15] J. D. Jorgensen, B. W. Veal, A. P. Paulikas, L. J. Nowicki, G. W. Crabtree, H. Claus, and W. K. Kwok, Phys. Rev. B **41**, 1863 (1990).
[16] A. M. Boffa and A. M. Cucolo, Int. J. Mod. Phys. B **14**, 2640 (2000).
[17] Z. Sefrioui, D. Arias, V. Peña, J. E. Villegas, M. Varela, P. Prieto, C. León, J. L. Martinez, and J. Santamaria, Phys. Rev. B **67**, 214511 (2003).
[18] J. Ye and K. Nakamura, Phys. Rev. B **48**, 7554 (1993).
[19] M. Varela, D. Arias, Z. Sefrioui, C. León, C. Ballesteros, S. J. Pennycook, and J. Santamaria, Phys. Rev. B **66**, 134517 (2002).
[20] P. Reutler, A. Bensaid, F. Herbstritt, C. Höfener, A. Marx, and R. Gross, Phys. Rev. B **62**, 11619 (2000).
[21] S. Wirth, A. Anane, B. Raquet, and S. von Molnár, J. Magn. Magn. Mater. **290-291**, 1168 (2005).

[22] J. M. D. Coey, M. Viret, L. Ranno, and K. Ounadjela, Phys. Rev. Lett. **75**, 3910 (1995).
[23] C. Martin, A. Maignan, M. Hervieu, B. Raveau, Z. J'írak, M. M. Savosta, A. Kurbakov, V. Trounov, G. André, and F. Bourée, Phys. Rev. B **62**, 6442 (2000).
[24] M. M. Savosta, P. Novák, M. Marysko, Z. J'írk, J. Hejtmánek, J. Englich, J. Kohout, C. Martin, and B. Raveau, Phys. Rev. B **62**, 9532 (2000).
[25] S. Machida, Y. Moritomo, S. Mori, N. Yamamoto, K. Ohoyama, E. Nishibori, and M. Takata, J. Phys. Soc. Jpn. **71**, 27 (2002).
[26] G. Alejandro, D. G. Lamas, L. B. Steren, J. E. Gayone, G. Zampieri, A. Caneiro, M. T. Causa, and M. Tovar, Phys. Rev. B **67**, 064424 (2003).
[27] G. B. Alers, A. P. Ramirez, and S. Jin, Appl. Phys. Lett. **68**, 3644 (1996).
[28] B. Raquet, A. Anane, S. Wirth, P. Xiong, and S. von Molnár, Phys. Rev. Lett. **84**, 4485 (2000).
[29] P. Levy *et al.*, J. Magn. Magn. Mater. **258-259**, 293 (2003).
[30] S. Hirano, J. Sugiyama, N. Tatsuo, and T. Tani, Phys. Rev. B **70**, 094419 (2004).
[31] J. Mira, J. Rivas, F. Rivadulla, C. Vázquez-Vázquez, and M. A. López-Quintela, Phys. Rev. B **60**, 2998 (1999).
[32] J. Moon-Ho, N. D. Mathur, J. E. Evetts, M. G. Blamire, M. Bibes, and J. Fontcuberta, Appl. Phys. Lett. **75**, 3689 (1999).
[33] C. M. Hurd, Contemp. Phys. **23**, 469 (1982).
[34] G. L. Squires, *Introduction to the Theory of Thermal Neutron Scattering* (Cambridge University Press, New York, 1978).
[35] A. R. Wildes, Rev. Sci. Instrum. **70**, 4241 (1999).
[36] S. Langridge, http://www.isis.rl.ac.uk/LargeScale/CRISP
[37] I. Felner, I. Nowik, I. Bradaric, and M. Gospodinov, Phys. Rev. B **62**, 11332 (2002).
[38] T. Nachtrab, C. Bernard, C. Lin, D. Koelle, and R. Kleiner, C. R. Phys. **7** (1), 68 (2006).